Simulation of Silicon Photomultiplier Signals

Stefan Seifert, Herman T. van Dam, Jan Huizenga, Ruud Vinke, Peter Dendooven, Herbert Löhner, *Member, IEEE*, and Dennis R. Schaart, *Member, IEEE*

***Abstract*—In a silicon photomultiplier (SiPM), also referred to as multi-pixel photon counter (MPPC), many Geiger-mode avalanche photodiodes (GM-APDs) are connected in parallel so as to combine the photon counting capabilities of each of these so-called microcells into a proportional light sensor. The discharge of a single microcell is relatively well understood and electronic models exist to simulate this process. In this paper we introduce an extended model that is able to simulate the simultaneous discharge of multiple cells. This model is used to predict the SiPM signal in response to fast light pulses as a function of the number of fired cells, taking into account the influence of the input impedance of the SiPM preamplifier. The model predicts that the electronic signal is not proportional to the number of fired cells if the preamplifier input impedance is not zero. This effect becomes more important for SiPMs with lower parasitic capacitance (which otherwise is a favorable property). The model is validated by comparing its predictions to experimental data obtained with two different SiPMs (Hamamatsu S10362-11-25u and Hamamatsu S10362-33-25c) illuminated with ps laser pulses. The experimental results are in good agreement with the model predictions.**

***Index Terms*—Equivalent circuit model, MPPC, non-proportionality, simulation, SiPM.**

I. Introduction

SILICON photomultipliers (SiPMs), also referred to as multi-pixel photon counters (MPPCs), are a relatively new and promising class of solid-state, low-level light sensors with potential in a multitude of applications such as high-energy physics, astronomy, biomolecular imaging, and medical imaging [1]–[4]. SiPMs are comprised of many, tiny, self-quenching Geiger-mode avalanche photodiodes (GM-APDs), all connected in parallel. A consequence of the Geiger-mode operation of the APDs is that their individual signals do not carry any information about the intensity of the detected light. However, the massive parallel connection of these so-called microcells, their small dimensions, their dense packaging, and their short recovery times (20 ns to 150 ns [5], [6]) allow for a nearly proportional response if the light intensity is not too high, i.e., if the probability that more than one photon hits a single microcell within its recovery time is negligible [7].

For a thorough analysis and interpretation of SiPM signals a detailed understanding of the discharge process and of the influence of the front-end electronics is compulsory. A powerful method to achieve this is the utilization of equivalent-circuit models that describe the physical discharge and quenching processes. Such models have already been developed for individual GM-ADPs [8], [9] and for single cells firing within a SiPM [10]–[12].

In this paper we introduce an extended model that allows for the simulation of the simultaneous firing of multiple microcells in a SiPM. We will show that such a multi-cell model is necessary to adequately describe the operation of a SiPM since its instantaneous electronic properties are a function of the number of cells firing. We will furthermore demonstrate that this results in an influence of the input impedance of the front-end electronics on the proportionality of the SiPM signal. The results obtained from these simulations are validated by comparison to experimental data obtained with two different SiPMs (Hamamatsu S10362-11-25u and Hamamatsu S10362-33-25c).

II. Methods and Materials

A. Simulation Model

The equivalent circuit simulating the discharge of N_{f} cells in a SiPM consisting of a total number of N_{tot} microcells is illustrated in Fig. 1. The dashed lines in Fig. 1 separate the circuit into an active part (left), representing a number of N_{f} fired microcells in parallel; a passive component (middle), representing the remaining, $N_{\mathrm{p}} = N_{\mathrm{tot}} - N_{\mathrm{f}}$ unfired microcells; and a parasitic capacitance C_{g} (right), which equals the sum of the parasitic capacitances of the N_{tot} cells connected in parallel. The resistor and capacitor values in the active and passive part of the circuit are given by

$$\begin{aligned} &C_{\mathrm{D,Nf}} = C_{\mathrm{D}} \cdot N_{\mathrm{f}},\ R_{\mathrm{q,Nf}} = \frac{R_{\mathrm{q}}}{N_{\mathrm{f}}},\ C_{\mathrm{q,Nf}} = C_{\mathrm{q}} \cdot N_{\mathrm{f}}, \\ &C_{\mathrm{D,Np}} = C_{\mathrm{D}} \cdot N_{\mathrm{p}},\ R_{\mathrm{q,Np}} = \frac{R_{\mathrm{q}}}{N_{\mathrm{p}}},\ C_{\mathrm{q,Np}} = C_{\mathrm{q}} \cdot N_{\mathrm{p}}, \\ &R_{\mathrm{D,Nf}} = \frac{R_{\mathrm{D}}}{N_{\mathrm{f}}} \end{aligned} \tag{1}$$

where C_{D} is the capacitance of the reverse-biased diode, R_{D} is the series resistance of the microplasma in the avalanche, R_{q} is the quench resistor and C_{q} is its associated stray capacitance, all for an individual microcell. For the special case of $N_{\mathrm{f}} = 1$ the equivalent circuit is similar to the ones used by Pavlov *et al.* [10] and Corsi *et al.* [11] to simulate the signal for a single fired cell in a SiPM.

In addition to the possibility to simulate signals for more than one fired cell, the circuit presented in Fig. 1 also differs from the latter two models in the way in which the signal charge is generated. Pavlov and Corsi both employ a current source, whilst in the present work the avalanche following a breakdown event

Manuscript received January 15, 2009; revised May 15, 2009. Current version published December 09, 2009. This work was supported by SenterNovem Grant IS055019.

S. Seifert, H. T. Van Dam, J. Huizenga, and D. R. Schaart are with Delft University of Technology, Delft 2629 JB, The Netherlands (e-mail: s.seifert@tudelft.nl).

R. Vinke, P. Dendooven, and H. Löhner are with the Kernfysisch Versneller Instituut (KVI), Groningen 9747 AA, The Netherlands.

Digital Object Identifier 10.1109/TNS.2009.2030728

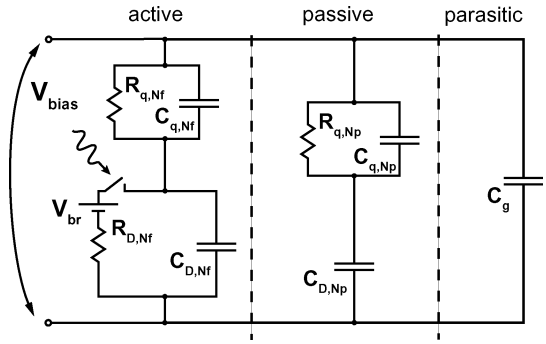

Fig. 1. Equivalent circuit for the discharge of N_{f} microcells in a SiPM (symbols are explained in Section II-A).

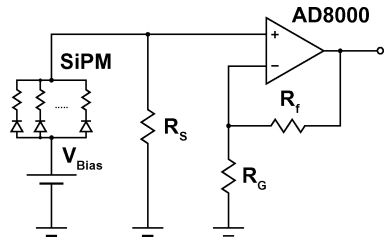

Fig. 2. Simplified diagram of the circuit used in the simulations and experiments. The circuit includes a voltage source V_{Bias} for SiPM biasing, the shunt resistor R_{S}, and a preamplifier based on the AD8000 opamp. Note that in this configuration V_{Bias} has to be negative to ensure that the SiPM is reverse biased.

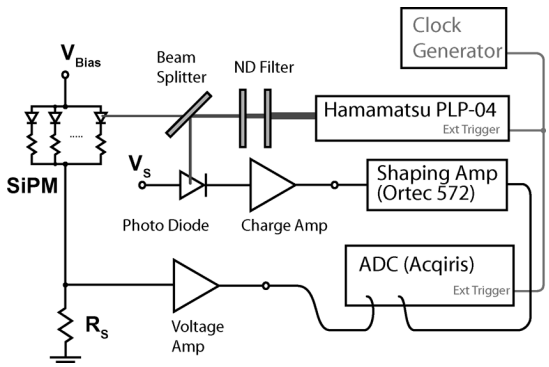

Fig. 3. The setup used to record the SiPM response to ps laser pulses. The reverse biased SiPM ($\mathrm{V_{Bias}} = -71.10\,\mathrm{V}$ for MPPC-11 and $\mathrm{V_{Bias}} = -68.82\,\mathrm{V}$ for MPPC-33) is illuminated with attenuated laser pulses. The signal is recorded over the shunt resistor R_{S} and digitized with a fast digitizer. Further details are given in the text.

is modeled by the voltage source V_{br}, the resistor R_{S}, and a switch. This is in accordance with the works by R. H. Haitz [8] and Cova *et al.* [9], which deal with breakdown events in individual diodes, rather than arrays of GM-APDs in a SiPM.

The switch is implemented such that it closes at a preset time t_0 marking the start of a breakdown event. The switch then monitors the microplasma current I_{D} through the diode (i.e., through R_{D} and V_{br}) and opens if I_{D} drops below a predefined threshold current $I_{\mathrm{q,Nf}}$, thus quenching the avalanche. $I_{\mathrm{q,Nf}}$ is determined by the average quenching current of an individual microcell I_{q} and the number of fired cells:

$$I_{\mathrm{q,Nf}} = I_{\mathrm{q}} \cdot N_{\mathrm{f}}. \tag{2}$$

B. Simulations

All electronic simulations in this work were performed with LTspice[1], a circuit simulation engine based on Berkeley SPICE 3f4[2]. In a first simulation aimed at the direct comparison of simulated and measured pulse traces, a transient analysis was performed on the circuit shown in Fig. 2. This circuit consists of the SiPM model discussed in Section II-A, a shunt resistor R_{S}, and a preamplification stage. The values of the shunt resistor and the resistors that determine the amplifier gain (R_{f} and R_{G} in Fig. 2), as well as the operational amplifier (opamp) type (AD8000 from Analog Devices) were chosen to match the ones used in the present experiments (see Section II-C). A SPICE model for the AD8000 opamp is available from the manufacturer. The model parameters for the SiPM electronic model were determined in separate experiments as described in Section II-D.

The influence of the shunt resistor R_{S} and the microplasma series resistance R_{D} on the SiPM signal was investigated in a second set of simulations. Here, the amplifier was omitted to exclude its potential influence on the signal (e.g., due to its finite bandwidth) and the signal charge was determined directly from the integral of the current through R_{S}.

In a third series of simulations, performed to derive the transfer function of a single cell, the switch was removed from the SiPM model and the voltage source was replaced by an ideal current source generating an AC signal. AC analyses in the frequency range between 100 kHz and 1 GHz were performed for different values of the shunt resistor R_{S}. Again, no amplifier was included. The -3 dB points were determined by linear interpolation between the two data points just above and below the -3 dB level. The error margin for this procedure is estimated as the distance between these two data points.

C. Experimental Setup

All experiments were performed with two different SiPMs, viz. the MPPC-S10362-11-25u and the MPPC-S10362-33-25c by Hamamatsu Photonics K.K. (denoted as MPPC-11 and MPPC-33, respectively, in the remainder of this work). The SiPMs were operated at $21^{\circ}\mathrm{C}$ and at a bias voltage of $V_{\mathrm{Bias}} = -71.10$ V in the case of the MPPC-11 and $V_{\mathrm{Bias}} = -68.82$ V in the case of the MPPC-33. These are the operating voltages recommended by the manufacturer, corresponding to 2.30 V (MPPC-11) and 1.52 V (MPPC-33) over breakdown (often also denoted as over-voltage). The dark count rates f_{d}, measured under these conditions are 250 kHz for the MPPC-11 and 2.2 MHz for the MPPC-33. f_{d} is defined here as the frequency of occurrence of a pulse with a peak height of least 0.5 times the average single cell signal. The cross talk and after pulsing probability at these conditions are reported to be 0.1% and 30%, respectively [13].

The setup used to determine the SiPM response to ps laser pulses is shown in Fig. 3. A SiPM was illuminated with a Hamamatsu PLP-04 laser (average pulse duration 50 ps, 10 kHz repetition rate). The laser light was fed via a fiber optic cable into a dark box. The diameter of the laser spot at the SiPM position was about 2 cm. The intensity of the light was regulated with

[1]http://www.linear.com/designtools/software/#Spice

[2]http://bwrc.eecs.berkeley.edu/Classes/icbook/SPICE/

neutral density filters. A 30%-to-70% beam splitter was used to couple a photodiode into the beam for monitoring the laser intensity.

The SiPM current was converted by a shunt resistor (R_{S}) into a voltage that was subsequently amplified by a high-bandwidth voltage amplifier (made in-house on the basis of the AD8000 current feedback opamp, see Fig. 2). This circuit layout was chosen because it allows for easy control of the impedance seen by the SiPM. The amplifier gain was adjusted to achieve similar output amplitudes with the two shunt resistors used in this work (287 V/A for $R_{\mathrm{S}} = 50\,\Omega$ and 295 V/A for $R_{\mathrm{S}} = 100\,\Omega$, respectively). The amplified signals were sampled using an Aqciris DC282 fast 10-bit digitizer at a sampling rate of 8 GS/s. The digitizer and the pulsed laser were simultaneously triggered by an external clock generator. Since both the amplifier gain and the value of R_{S} were known, the signal charge could be determined from the integral of the recorded trace. The time window for the integration Δt_{i} was chosen to match the SiPM pulses ($\Delta t_{\mathrm{i}} = 40$ ns for MPPC-11 and $R_{\mathrm{S}} = 50\,\Omega$; $\Delta t_{\mathrm{i}} = 60$ ns for MPPC-11 and $R_{\mathrm{S}} = 100\,\Omega$; $\Delta t_{\mathrm{i}} = 120$ ns for MPPC-33 and $R_{\mathrm{S}} = 50\,\Omega$; and $\Delta t_{\mathrm{i}} = 210$ ns for MPPC-33 and $R_{\mathrm{S}} = 100\,\Omega$).

In experiments in which the laser intensity was of interest, the signal of the abovementioned photodiode was shaped using an Ortec 572A shaping amplifier (shaping time 500 ns, gain 25) and the shaped signal was digitized simultaneously with the SiPM signal using the same digitizer. In these cases the sample rate for both signals was reduced to 4 GS/s.

D. Determination of the Model Parameters

The input parameters for the model described in Section II-A were determined for each of the two SiPMs. Since the total number of microcells is known for both devices (1600 for the MPPC-11 and 14400 for the MPPC-33, respectively), the value of R_{q} can readily be obtained from the IV-curve of the forward-biased SiPM.

The sum of the two capacitors C_{q} and C_{D} can be determined if the charge Q_{C} per fired cell and the breakdown voltage V_{BR} are known [9]:

$$\begin{aligned} Q_{\mathrm{C}} &= \frac{R_{\mathrm{q}}}{R_{\mathrm{q}} + R_{\mathrm{D}}}(V_{\mathrm{bias}} - V_{\mathrm{BR}})(C_{\mathrm{D}} + C_{\mathrm{q}}) \\ &\approx (V_{\mathrm{bias}} - V_{\mathrm{BR}})(C_{\mathrm{D}} + C_{\mathrm{q}}). \end{aligned} \tag{3}$$

For a fixed bias voltage, Q_{C} can be obtained by applying a linear fit to the peak positions in a signal charge histogram recorded at low light intensity (see Fig. 4 for an example) with the setup described in Section II-B. V_{BR} can be determined by repeating these measurements at different bias voltages and extrapolating $Q_{\mathrm{C}}(V_{\mathrm{BR}})$ to zero.

A procedure to separate the sum of the capacitances C_{D} and C_{q} into its individual components and to determine C_{g} has been given by Corsi *et al.* [11]. The complex impedance $Z(\omega)$ of the reverse-biased SiPM is measured in a dark box with a precision LCR meter (Agilent 4282A) at a signal frequency of $\omega = 1$ MHz. Since the bias applied (-40 V) is well below the breakdown voltage, no cells are fired and the equivalent circuit

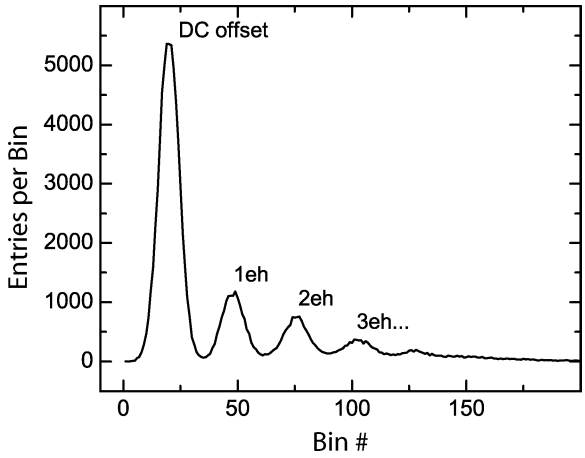

Fig. 4. Signal charge histogram measured with MPPC-11 at a bias voltage of -71.10 V showing single, double, and triple electron–hole (eh) pair peaks. The bin size is 1.7 fC.

for the SiPM is reduced to the passive (plus parasitic) component with $N_{\mathrm{p}} = N_{\mathrm{tot}}$, see Fig. 1 and (1). $Z(\omega)$ can then be expressed as:

$$\begin{aligned} Z^{-1}(\omega) &= \left(\frac{1}{G_\omega} \| \frac{1}{i\omega C_\omega}\right)^{-1} = G_\omega + i\omega C_\omega \\ &= \left[\left(R_{\mathrm{q,Np}} \| 1/i\omega C_{\mathrm{q,Np}} + \frac{1}{i\omega C_{\mathrm{D,Np}}}\right) \| \frac{1}{i\omega C_{\mathrm{g}}}\right]^{-1} \end{aligned} \tag{4}$$

where G_ω and C_ω are the measured parallel conductance and capacitance of the SiPM, respectively, at the signal frequency ω. Equation (4) can be rewritten to derive the following expressions[3] for C_{D} and C_{g}:

$$C_{\mathrm{D}} = \sqrt{\frac{1 + \omega^2 (C_{\mathrm{D}} + C_{\mathrm{q}})^2 R_{\mathrm{q}}^2}{\omega^2 N_{\mathrm{tot}} R_{\mathrm{q}}} \cdot G_\omega} \tag{5}$$

$$C_{\mathrm{g}} = C_\omega - N_{\mathrm{tot}} C_{\mathrm{D}} + \frac{\omega^2 {C_{\mathrm{D}}}^2 R_{\mathrm{q}}^2 N_{\mathrm{tot}} (C_{\mathrm{D}} + C_{\mathrm{q}})}{1 + \omega^2 R_{\mathrm{q}}^2 (C_{\mathrm{D}} + C_{\mathrm{q}})^2}. \tag{6}$$

III. Results and Discussion

A. SiPM Model Parameters

The model parameters determined for MPPC-11 and MPPC-33 are summarized in Table I. The measured capacitance of the individual diodes and the quench resistors' stray capacitance are similar for the two SiPMs investigated. This is expected, as the pitch between the microcells and the area of the diodes are the same for both devices. However, the nine times larger total area of MPPC-33 results in a parasitic capacitance much larger than that of MPPC-11.

A value for the average quenching current I_{q} is not readily available through measurement on a SiPM. Yet, a reasonable estimate can be made based on the quench resistor values and

[3]The equations for C_{D} and C_{g} as published in [11] contain two errors. Firstly the denominator under the square root in (5) contains R_{q}^2 instead of R_{q}, which would leave this equation with unbalanced units. Secondly the sign of the last term in (6) is reversed.

TABLE I
SUMMARY OF THE MODEL PARAMETERS DETERMINED EXPERIMENTALLY FOR MPPC-11 AND MPPC-33. THE ERROR MARGINS INDICATE 95% CONFIDENCE INTERVALS

		MPPC-11	MPPC-33
V_{br}	(V)	68.8 ± 1.5	67.3 ± 0.9
C_{D}	(fF)	15.0 ± 1.2	15.4 ± 0.4
C_{q}	(fF)	4.3 ± 1.2	3.4 ± 0.4
R_{q}	(kΩ)	179 ± 1	268 ± 2
C_{g}	(pF)	7.5 ± 1.9	59 ± 5
R_{d}	(kΩ)	1	1
I_{q}	(μA)	30	30

the voltage over breakdown V_{OB} during normal operation of the device.

After an avalanche is triggered, the initially large microplasma current will drop and approach an asymptotic value I_{f} due to the presence of the quench resistor [9]:

$$I_{\mathrm{f}} = \frac{V_{\mathrm{OB}}}{R_{\mathrm{q}} + R_{\mathrm{D}}} \approx \frac{V_{\mathrm{OB}}}{R_{\mathrm{q}}}. \tag{7}$$

where the approximation is justified since R_{q} typically has a value of several hundred kΩ while R_{D} lies within the range between 500 Ω and a few kΩ [9].

For the operation of a SiPM it is imperative, that every avalanche is quenched properly and therefore R_{q} must be chosen such that I_{f} is well below I_{q}. On the other hand, R_{q} should be chosen as small as possible to ensure fast recovery times. Therefore, I_{q} should be larger, but not much larger than I_{f} in a properly designed SiPM. Using the values presented in Table I, I_{f} can be calculated to be 13 μA for the MPPC-11 and 6 μA for the MPPC-33. Based on these values, I_{q} was set to 30 μA. This value was chosen for both detectors, since the individual GM APDs that compose the two devices should essentially be the same.

The determination of the microplasma series resistance R_{D} poses a similar problem. Since a direct measurement of the voltage drop over a diode within an individual microcell is not feasible, the only remaining possibility is a determination from the signal rise time τ_{r}, via the relation [9]

$$\begin{aligned}\tau_{\mathrm{r}} &= (C_{\mathrm{D,Nf}} + C_{\mathrm{q,Nf}}) \cdot \frac{R_{\mathrm{D,Nf}} \cdot R_{\mathrm{q,Nf}}}{R_{\mathrm{D,Nf}} + R_{\mathrm{q,Nf}}} \\ &= (C_{\mathrm{D}} + C_{\mathrm{q}}) \cdot \frac{R_{\mathrm{D}} \cdot R_{\mathrm{q}}}{R_{\mathrm{D}} + R_{\mathrm{q}}} \\ &\approx (C_{\mathrm{D}} + C_{\mathrm{q}}) \cdot R_{\mathrm{D}}. \end{aligned} \tag{8}$$

There are, however, additional factors influencing the rise time of the measured signal, such as the finite bandwidth of the amplifier and the digitizer as well as inductances in the signal chain, which prevent a direct extraction of the value of R_{D}. For all matters discussed in this work, however, the influence of R_{D} is very small. Fig. 5 illustrates that varying R_{D} within a range of 500 Ω to 5 kΩ has only very little effect on the simulated signal shape. This also underlines the difficulty of determining R_{D} from a measured signal. In Fig. 6 the signal charge obtained from the simulated data, using $N_{\mathrm{f}} = 1000$ for MPPC-11 and $N_{\mathrm{f}} = 5000$ for MPPC-33, is plotted as a function of R_{D}. The output signal charge is expressed in terms of the equivalent

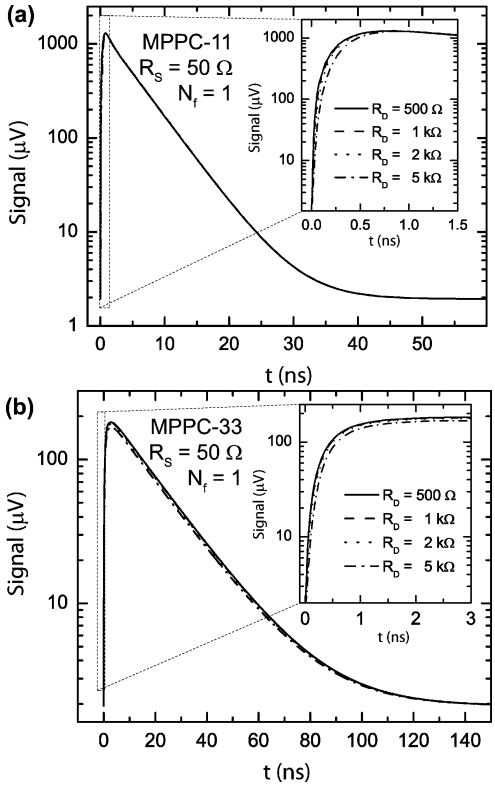

Fig. 5. Simulated signal as a function of the microplasma series resistance. For both devices, (a) the MPPC-11 and (b) the MPPC-33, the observed changes are marginal when varying R_{D} from 500 Ω to 5 kΩ. The insets show the initial parts of the pulses.

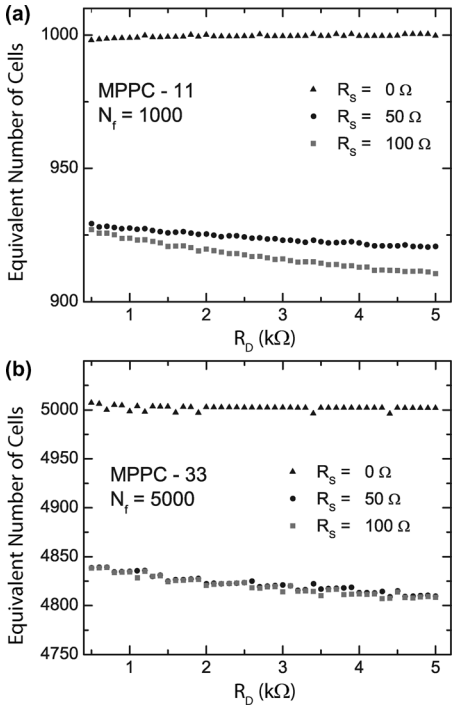

Fig. 6. Equivalent number of fired cells $N_{\mathrm{f}}^{\mathrm{e}}$ obtained from the simulated data, for a true number of fired cells $N_{\mathrm{f}} = 1000$ for MPPC-11(a) and for $N_{\mathrm{f}} = 5000$ for MPPC-33 (b), as a function of R_{D}.

number of fired cells $N_{\mathrm{f}}^{\mathrm{e}}$, defined as the ratio of the total signal charge and the charge due to a single firing microcell. Also in

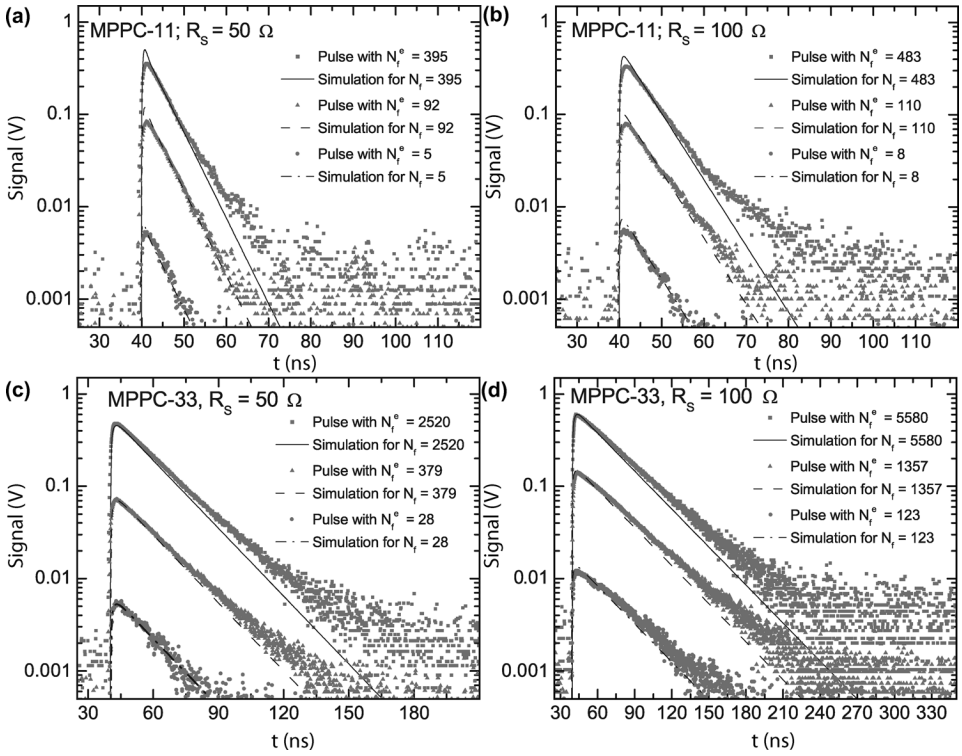

Fig. 7. Examples of simulated and measured pulse traces of the two SiPMs in combination with different shunt resistors, illuminated with ~ 50 ps laser pulses of different intensity: MPPC-11 and $R_{\rm S} = 50\ \Omega$ (a), MPPC-11 and $R_{\rm S} = 100\ \Omega$ (b), MPPC-33 and $R_{\rm S} = 50\ \Omega$ (c), MPPC-33 and $R_{\rm S} = 100\ \Omega$ (d). The equivalent number of fired cells was calculated from the pulse integrals and the single cell gain.

this figure, the change with $R_{\rm D}$ is small, compared to the deviation of the measured $N_{\rm f}^{\rm e}$ from $N_{\rm f}$ with increasing shunt resistor $R_{\rm S}$. The latter effect will be discussed later on in this paper. In the remaining simulations presented in this work a value of 1 kΩ was assumed for $R_{\rm D}$.

B. Comparison of Simulations and Measured Data

Fig. 7 shows some experimentally recorded traces for different combinations of SiPMs and shunt resistors and for different laser intensities. These are compared to traces simulated for the same conditions and with $N_{\rm f}$ matching the equivalent number of fired cells obtained from the pulse integral of the corresponding measured trace. The figure shows that both pulse height and pulse shape are reproduced quite well by the simulations, especially around the initial decay of the pulses. These parts of the traces are governed by the low-pass characteristics of the circuit formed by the combination of the SiPM and the shunt resistor. The -3 dB point of this low pass filter can be obtained from the simulated transfer function of the circuit (SiPM model plus $R_{\rm S}$). The time constant $\tau_{-3{\rm dB}}$ corresponding to the frequency at the -3 dB point $f_{-3{\rm dB}}$ then corresponds very well to the pulse decay times $\tau_{\rm d}$ obtained by fitting an exponential function to the measured curve (see Table II). The error margins for $\tau_{\rm d}$ were estimated from the 95% confidence intervals of the fits to the measured data.

Starting from about 20 ns – 50 ns after the light pulse, however, the measured traces start to deviate from the predicted ones. This can be attributed to afterpulsing of some of the fired cells, which is not taken into account by the simulations and which leads to the observed slower decay.

TABLE II
COMPARISON OF THE MEASURED SIPM SIGNAL DECAY TIME $\tau_{\rm d}$ AND THE CHARACTERISTIC TIME CONSTANTS ASSOCIATED WITH THE -3 dB POINTS IN THE SIPM SIGNAL TRANSFER FUNCTIONS

	MPPC-11		MPPC-33	
	$R_{\rm S} = 50\ \Omega$	$R_{\rm S} = 100\ \Omega$	$R_{\rm S} = 50\ \Omega$	$R_{\rm S} = 100\ \Omega$
$\tau_{\rm d}$ (ns)	4.66 ± 0.12	5.92 ± 0.16	18.55 ± 0.20	34.13 ± 0.16
$f_{-3{\rm dB}}$ (MHz)	34.52 ± 0.08	26.50 ± 0.07	8.95 ± 0.022	5.03 ± 0.012
$\tau_{-3{\rm dB}}$ (ns)	4.61 ± 0.011	6.00 ± 0.016	17.78 ± 0.05	31.66 ± 0.08

A slight mismatch also remains in the rising edges, which, in all measurements, is somewhat slower than predicted by the simulations (see Table III). There are a number of potential reasons for this mismatch. One possibility is the presence of inductances in the signal chain which limit the bandwidth of the overall circuit. Simulations with a modified SiPM model show that an inductance of a few nH in series with the SiPM could already decrease the rise time to the observed value. A second possible reason is that differences between the signal transient times of different microcells could lead to an increase in the effective signal rise time, as the signals from many fired cells are being summed. These differences, however, are expected to be in the order of a few hundred ps due to the relatively small dimensions of the devices and are therefore expected to be too small to be the sole reason for the observed increase in rise time. Thirdly, also the choice of $R_{\rm D}$ has some influence on the simulated signal rise times. However, this influence is small for a large range of resistor values (see Fig. 6).

TABLE III
COMPARISON OF THE 10%-90% RISE TIME OBTAINED FROM THE MEASURED DATA ($t_{\mathrm{m}}^{10\text{-}90}$) AND FROM THE SIMULATED TRACES ($t_{\mathrm{s}}^{10\text{-}90}$)

	MPPC-11		MPPC-33	
	$R_{\mathrm{S}} = 50\ \Omega$	$R_{\mathrm{S}} = 100\ \Omega$	$R_{\mathrm{S}} = 50\ \Omega$	$R_{\mathrm{S}} = 100\ \Omega$
$t_{\mathrm{m}}^{10\text{-}90}$ (ns)	1.2 ± 0.2	1.2 ± 0.2	2.0 ± 0.2	2.2 ± 0.2
$t_{\mathrm{s}}^{10\text{-}90}$ (ns)	0.4 ± 0.05	0.5 ± 0.05	1.2 ± 0.05	1.4 ± 0.05

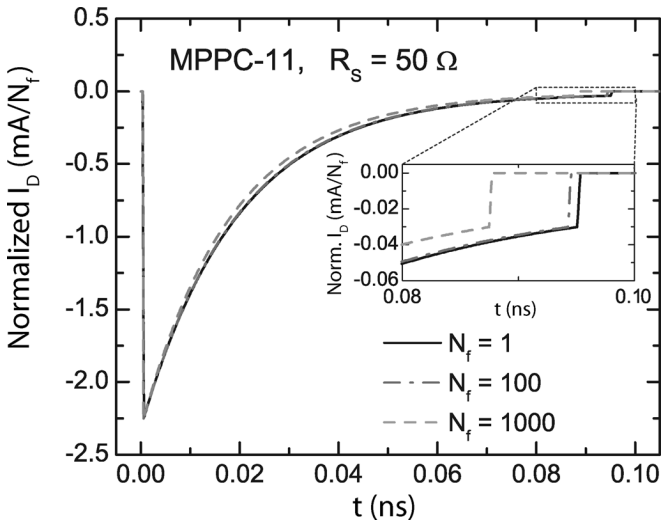

Fig. 8. Simulated microplasma current I_{D} for different N_{f}. I_{D} is normalized to N_{f}. The inset depicts a zoom on the tail of the pulses, where the avalanches are quenched.

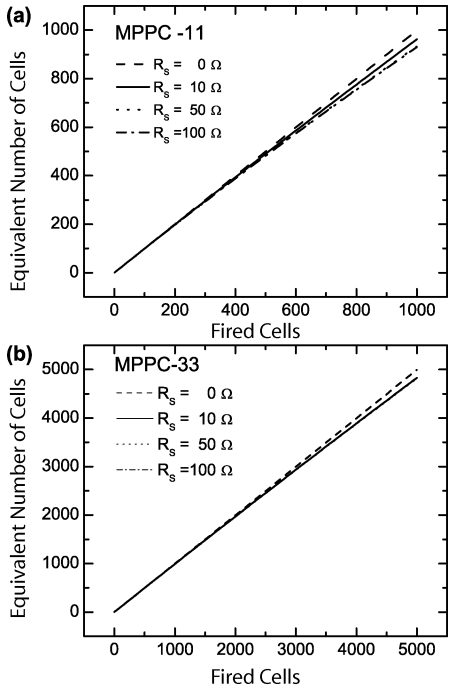

Fig. 9. Predicted SiPM signal, normalized to the single cell charge, as a function of the true number of fired cells, for (a) MPPC-11 and (b) MPPC-33. Both SiPMs show an increasing deviation of the equivalent number of fired cells from the true value of N_{f} with increasing N_{f}. Please note that the lines for $R_{\mathrm{S}} = 50\ \Omega$ and $R_{\mathrm{S}} = 100\ \Omega$ overlap in both figures.

A further prediction of the model concerns the signal generation. The parallel combination of firing microcells leads to a decrease of both $R_{\mathrm{q,Nf}}$ and $R_{\mathrm{D,Nf}}$ with increasing number of fired cells. Since both resistors decrease at the same rate, the ratio between $R_{\mathrm{D,Nf}}$ and the quench resistor also remains constant, as long as the load impedance is zero. This, however, changes, when the resistor R_{S} is added in series. Now, an increase in the number of fired cells changes the ratio between $R_{\mathrm{D,Nf}}$ and the effective quench resistor $R_{\mathrm{q,Nf}} + R_{\mathrm{S}}$. The resulting effect is the same, as if the quench resistor of the individual cells was increased. The result is an earlier average quenching time. This is illustrated in Fig. 8, where the normalized microplasma current I_{D} is shown for an increasing number of fired cells.

It should be noted, that the time constant associated with the decay of the avalanche current is mainly determined by R_{D} (since $R_{\mathrm{D,Nf}} \ll R_{\mathrm{q,Nf}} + R_{\mathrm{S}}$ remains true, also for larger N_{f}). Therefore, it may not be immediately obvious why the quenching threshold should be reached earlier as N_{f} increases. The answer lies in the fact that the avalanche current does not decay to zero but to the asymptotic value given in (7), which is governed by the quench resistor value. As the quench resistor effectively increases, this asymptotic value decreases, and since the avalanche decays towards a lower asymptotic value, it reaches the quenching threshold on average earlier.

The decrease of the average quenching time with increasing N_{f} decreases the charge per fired cell and, therefore, the signal is no longer proportional to N_{f}. This behavior is illustrated in Fig. 9, which shows the simulated output signal as a function of the number of fired cells for different shunt resistor values R_{s}. Both SiPMs exhibit a distinct deviation from proportionality if the input impedance of the front-end electronics is not zero. This electronic non-proportionality is most pronounced for MPPC-11: at 1000 fired cells and with $R_{\mathrm{S}} = 50\ \Omega$ the deviation is 7%, compared to only 1% for MPPC-33 under the same conditions.

This difference between the two SiPMs is examined in more detail in Fig. 10, in which the equivalent number of fired cells $N_{\mathrm{f}}^{\mathrm{e}}$ is plotted against R_{S} for a fixed number of fired cells ($N_{\mathrm{f}} = 1000$). For both SiPMs, $N_{\mathrm{f}}^{\mathrm{e}}$ decreases quickly as R_{S} is increased above zero, until an asymptotic value is approached. In Fig. 10(a) it is apparent that this happens at much lower R_{S} for MPPC-33 than for MPPC-11. One cause of this difference is the difference in total SiPM capacitance. The capacitances of MPPC-11 and MPPC-33 can be estimated from the values given in Table I to be $\sim$ 11 pF and $\sim$ 99 pF, respectively, at high frequencies, and $\sim$ 32 pF and $\sim$ 281 pF, respectively, at low frequencies. The SiPM capacitance, however, constitutes a finite impedance at any of the frequencies within the signal spectrum and, since it is in parallel to R_{S}, this impedance limits the shunt resistor's influence on the quenching process. This can be illustrated by increasing the parasitic capacitance C_{g} (and thus the total capacitance) in the MPPC-11 model. Fig. 10(b) shows that this leads to a significant reduction of the observed non-proportionality indeed.

A second reason for the electronic non-proportionality to be more pronounced for MPPC-11 than for MPPC-33 is the fact that MPPC-11 has a smaller quench resistor value R_{q} (see Table I). This means that, relative to R_{q}, the increase of the

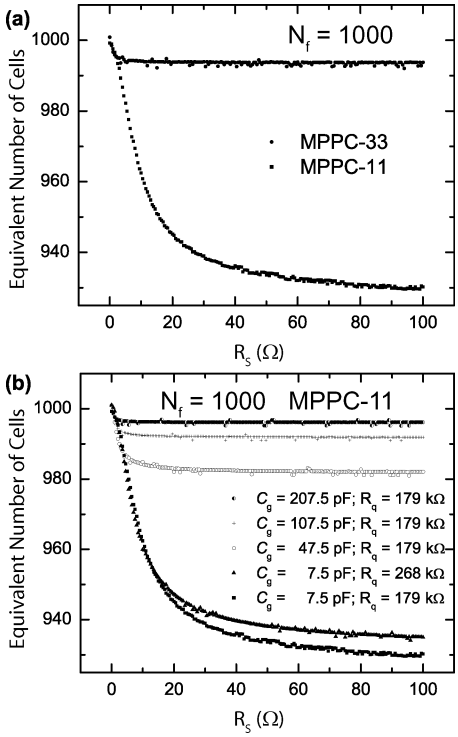

Fig. 10. SiPM signal, normalized to the single cell charge plotted against R_{S} for MPPC-11 at a fixed number of 1000 fired cells (a) in comparison to MPPC-33 and (b) as a function of C_{g} and for two different values for $R\mathrm{q}$ (179 $\mathrm{k}\Omega$, corresponding to MPPC-11, and 268 $\mathrm{k}\Omega$, corresponding to MPPC-33, respectively).

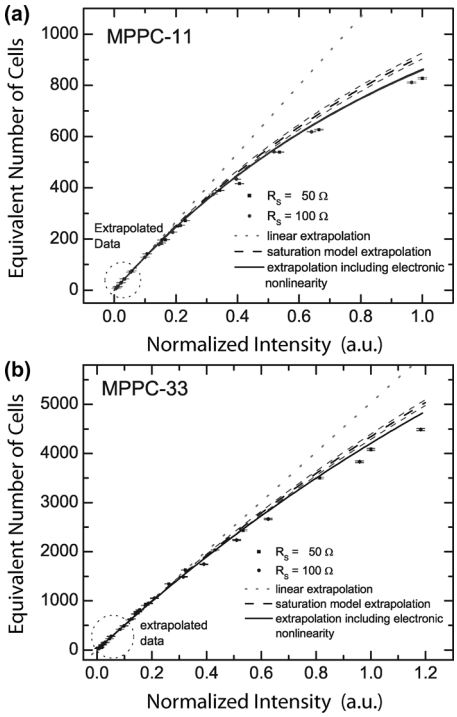

Fig. 11. Signals of (a) MPPC-11 and (b) MPPC-33 plotted against the relative intensity of the exciting laser pulse. The dotted red line is a linear extrapolation of the data points at the low light intensity. The dashed line constitutes the extrapolation of the SiPM signals below 80 (MPPC-11) and 500 (MPPC-33) equivalent fired cells with the corresponding 95% prediction intervals, taking into account optical SiPM saturation. The solid lines depict the correction of the extrapolated curve for the electronic non-proportionality.

effective quench resistance with N_{f} is larger if all other conditions are the same. This is demonstrated by changing R_{q} in the MPPC-11 model from 179 $\mathrm{k}\Omega$ to 268 $\mathrm{k}\Omega$ (i.e., the value for the MPPC-33. This slightly reduces the electronic non-proportionality indeed. As can be seen in Fig. 10(b), however, this effect is much smaller than the change due to the added capacitance.

The predicted electronic non-proportionality can also be found in the experimental data. In Fig. 11 the signals of MPPC-11 (a) and MPPC-33 (b) are plotted against the intensity of the exciting laser pulses for two different shunt resistor values. For each data point in this figure, both the signal charge and the laser pulse intensity were averaged over at least 2000 pulses.

Unfortunately, the interpretation of these measurements is complicated by the intrinsic non-proportionality of the SiPM response to optical stimulation [7]. However, for light pulses of much shorter duration than the GM-APD recharge time a simple statistical model can be used to describe the relationship between the number of fired cells N_{f} and the intensity of the exciting light pulse [7]:

$$N_{\mathrm{f}} = N_{\mathrm{tot}}\left[1 - \exp\left(-\frac{\xi \cdot I}{N_{\mathrm{tot}}}\right)\right] \tag{9}$$

where ξ is the constant of proportionality between the measured laser intensity I and the number of triggered cells, given that all cells are fully charged at the time. It is comprised of the photon detection efficiency of the device, the cross talk probability and a constant of proportionality between I and the number of photons arriving at the sensor. ξ can be determined by fitting this saturation model to the experimental data. Since (9) does not take into account electronic non-proportionality, the fit was performed using only the data points corresponding to up to 80 equivalent fired cells for MPPC-11 and up to 500 equivalent fired cells for MPPC-33 (as indicated by the dotted circles in Fig. 11). In this range the calculated electronic non-proportionality is smaller than 0.5% for both detectors.

Extrapolation of these fits (dashed lines in Fig. 11) shows that the measured signals for both SiPMs and for both shunt resistor values are indeed smaller than would be expected if only optical SiPM saturation were considered. Also the fact that the observed deviation is much stronger for the smaller MPPC-11 with smaller associated capacitance is in agreement with our model. Here it should be noted that the same procedure applied to data obtained with a transimpedance amplifier with very low input impedance yielded good agreement between the extrapolation and the measured data [14].

The solid lines in Fig. 11 depict the correction of the extrapolation of N_{f} for the electronic non-proportionality, as predicted by the simulations. The graphs indicate that the simulations actually underestimate the magnitude of the electronic non-proportionality. This might be linked, again, to the neglected inductances of the SiPM and of the electronics used in the experiments. Inductances in the signal chain can increase the impedance at signal frequencies, which in return would increase the deviation from proportionality. This is plausible since the impedance seen by the SiPM in the signal frequency

band is only a few Ω, so small absolute changes can have a large influence on the observed behavior.

IV. Conclusions and Outlook

An improved electronic model for the simulation of the simultaneous firing of multiple microcells in a SiPM has been introduced in this paper. The necessary model parameters were determined experimentally for two different SiPMs (Hamamatsu S10362-11-25u and Hamamatsu S10362-33-25c). Comparison of simulated and measured signals of these SiPMs was shown to yield excellent agreement.

Furthermore, it is shown that the model can be an important tool for the interpretation of the SiPM response to instantaneous light pulses and for the development of front-end electronics. This was illustrated by predicting the effect of the preamplifier input impedance on the proportionality of the SiPM signal. The electronic signal was shown to be non-proportional to the number of fired cells unless the preamplifier input impedance equals zero. Again, these predictions were confirmed by experiments.

Although the assumption of simultaneous triggering of the microcells might seem a limitation of the proposed multicell model, its practical use is not necessarily limited to the case of instantaneous excitation. In fact, the model can easily be adapted to simulate the response to a light pulse of finite duration (such as a scintillation pulse). This can be done by placing a number of active subcircuits in parallel and closing the corresponding switches according to a predefined trigger schedule determined by the probabilities of photon arrival and absorption, avalanche triggering, crosstalk and afterpulsing (which can e.g., be obtained by Monte Carlo simulation).

Each of the active subcircuits may represent any number of fired cells, which allows for a grouping of cells that may greatly reduce the necessary number of circuit elements and thus the computational expense of such a simulation. Cells may be grouped if they a) are fired within a small time window (smaller then the avalanching time) and b) are not fired again until they are completely recharged. If the second condition is not met for a given cell, it could be treated as a single cell in order to properly account for the influence of the cell recovery time on subsequent discharges. The realization of such a model and an investigation as to how accurately it predicts recovery times and scintillation pulses is currently in progress.

References

[1] G. Bondarenko *et al.*, "Limited Geiger-mode microcell silicon photodiode: New results," *Nucl. Instrum. Methods Phys. Res. A*, vol. 442, pp. 187–192, 2000.

[2] P. Buzhan *et al.*, "Silicon photomultiplier and its possible applications," *Nucl. Instrum. Methods Phys. Res. A*, vol. 504, pp. 48–52, 2003.

[3] B. Dolgoshein *et al.*, "Status report on silicon photomultiplier development and its applications," *Nucl. Instrum. Methods Phys. Res. A*, vol. 563, pp. 368–376, 2006.

[4] A. N. Otte *et al.*, "A test of silicon photomultipliers as readout for PET," *Nucl. Instrum. Methods Phys. Res. A*, vol. 545, pp. 705–715, 2005.

[5] S. Uozumi, "Study and development of multi pixel photon counter for the GLD calorimeter readout," in *Proc. Int. Workshop on New Photon-Detectors 2007 (PD07)*, Kobe, Japan, 022.

[6] K. C. Burr and G.-C. Wang, "Scintillation detection using 3 mm $\times$ 3 mm silicon photomultipliers," in *IEEE Nucl. Sci. Symp. Conf. Rec., 2007 (NSS '07)*, Honolulu, HI, pp. 975–982, N18-2.

[7] P. Buzhan *et al.*, "An advanced study of silicon photomultiplier," *ICFA Instumentation Bulletin*, vol. 23, pp. 28–42, 2001.

[8] R. H. Haitz, "Model for the electrical behavior of a microplasma," *J. Appl. Phys.*, vol. 35, pp. 1370–1376, May 1964.

[9] S. Cova, M. Ghioni, A. Lacaita, C. Samori, and F. Zappa, "Avalanche photodiodes and quenching circuits for single-photon detection," *Appl. Opt.*, vol. 35, pp. 1956–1976, Apr. 1996.

[10] N. Pavlov, G. Mæhlum, and D. Meier, "Gamma spectroscopy using a silicon photomultiplier and a scintillator," in *IEEE Nucl. Sci. Symp. Conf. Rec. 2005*, Puerto Rico, 2005, pp. 173–180, N9-3.

[11] F. Corsi *et al.*, "Modelling a silicon photomultiplier (SiPM) as a signal source for optimum front-end design," *Nucl. Instrum. Methods Phys. Res. A*, vol. 572, pp. 416–418, 2007.

[12] K. A. Wangerin, G.-C. Wang, C. Kim, and Y. Danon, "Passive electrical model of silicon photomultipliers," in *IEEE Nucl. Sci. Symp. Conf. Rec., NSS '08*, Dresden, Germany, pp. 4906–4913, M10-202.

[13] K. Yamamoto *et al.*, "Development of multi-pixel photon counter (MPPC)," in *IEEE Nucl. Sci. Symp. Conf. Rec., NSS '07*, Honolulu, HI, pp. 1511–1515, N24-292.

[14] S. Seifert *et al.*, "A high bandwidth preamplifier for SiPM-based TOF PET scintillation detectors," in *IEEE Nucl. Sci. Symp. Conf. Rec., NSS '08*, Dresden, Germany, pp. 1616–1619, NM1-2.